Infrared and Optical Properties of β'-$(ET)_2SF_5CF_2SO_3$: Evidence for a 45 K Spin-Peierls Transition

J. M. Pigos, B. R. Jones, Z.-T. Zhu, and J. L. Musfeldt*

Department of Chemistry, State University of New York at Binghamton, Binghamton, New York 13902-6016

C. C. Homes

Department of Physics, Brookhaven National Laboratory, Upton, New York 11793

H.-J. Koo and M.-H. Whangbo

Department of Chemistry, North Carolina State University, Raleigh, North Carolina 27695-8204

J. A. Schlueter, B. H. Ward, H. H. Wang, and U. Geiser

Chemistry and Materials Science Divisions, Argonne National Laboratory, Argonne, Illonois 60439

J. Mohtasham, R. W. Winter, and G. L. Gard

Department of Chemistry, Portland State University, Portland, Oregon 97207-0751

Received October 20, 2000. Revised Manuscript Received January 24, 2001

We measured the polarized infrared reflectance of β'-$(ET)_2SF_5CF_2SO_3$ as a function of temperature and analyzed the spin-exchange interactions of this salt by calculating the spin−orbital interaction energies between adjacent spin sites. The observed changes in vibrational properties below the 45 K transition support a weak lattice distortion in combination with a spin gap in this material. The spin-exchange interaction is predicted to occur primarily along the $(-a+b)$ diagonal direction, in good agreement with the spectral data. In addition, notable frequency shifts of vibrational modes point to a second transition between 100 and 200 K. The low-lying electronic excitation in the stack direction (assigned as a charge-transfer feature based upon our electronic band structure calculations) shows distinct changes with temperature that are consistent with trends in the vibrational spectrum. The pattern of a high-temperature transition preceding the spin-Peierls transition is discussed in relation to other low-dimensional organic and inorganic materials.

I. Introduction

Recently, there has been a great deal of interest in low-dimensional magnetic solids. In particular, the magnetoelelastic spin-Peierls (SP) transition has attracted attention. Several examples of SP coupling have been observed in organic and inorganic systems alike. Organic compounds, such as (TTF) M (BDT): M = Cu,Au, MEM$(TCNQ)_2$ and $(TMTTF)_2$ PF_6 display SP transitions at $T_{SP} = 12$ (2) for M = Cu(Au), 18, and 20 K, respectively.[1,2] More recently, transition metal oxides such as $CuGeO_3$ ($T_{SP} \approx 14$ K), the $S = 1$ chain material $LiVGe_2O_6$ ($T_{SP} \approx 22$ K), and a related compound α'-NaV_2O_5 ($T_{SG} \approx 35$ K, where SG = spin gap), have been found to display interesting magnetic properties.[3−5]

β'-$(ET)_2SF_5CF_2SO_3$ (ET = bis(ethylenedithio)tetrathiafulvalene) is a recently developed organic salt that has been predicted to undergo a SP transition.[6] With an oxidation state of +0.5 for ET, each dimer forms an $(ET)_2^+$ cation that has one unpaired spin. This dimer can act as a spin site. Theoretical work has predicted a magnetoelastic pairing of these spins to form a SP ground state.[6] Preliminary evidence for a SP transition was observed in both electron spin resonance (ESR) line width and relative magnetic susceptibility measurements. High-field ESR work supports these findings

* To whom correspondence should be addressed. Current address: Department of Chemistry, University of Tennessee, Knoxville, TN 37996.

(1) Bray, J. W.; Interrante, L. V.; Jacobs, I. S.; Bonner, J. C. *Extended Linear Chain Compounds*; Miller, S., Ed.; Plenum: New York, 1983; Vol. 3.

(2) TTF is tetrathiafulvalene and BDT is bis-dithiolene; MEM is *N*-methyl-*N*-ethylmorpholinium and TCNQ is tetracyanoquinodimethane; TMTTF is tetramethyltetrathiafulvalene.

(3) Hase, M.; Terasaki, I.; Uchinokura, K. *Phys. Rev. Lett.* **1993**, *70*, 3651.

(4) Musfeldt, J. L. *Magnetism*: *From Molecules to Materials*; Miller, J. S., Drillon, M., Eds.; VCH−Wiley: in press.

(5) Millet, J.; Mila, F.; Zhang, F. C.; Mambrini, M.; Van Oosten, A.; Pashchenko, V. A.; Sulpice, A.; Stepanov, A. *Phys. Rev. Lett.* **1999**, *83*, 4176.

(6) Ward, B. H.; Schlueter, J. A.; Geiser, U.; Wang, H. H.; Morales, E.; Parakka, J.; Thomas, S. Y.; Williams, J. M.; Nixon, P. G.; Winter, R. W.; Gard, G. L.; Koo, H.-J.; Whangobo, M.-H. *Chem. Mater.* **2000**, *12*, 343.

10.1021/cm000839d CCC: $20.00
Published on Web 03/02/2001

with an isotropic drop of the susceptibility, yielding a spin gap of $\triangle \approx 114$ K using BCS mean-field theory.[7] More recent (and still ongoing) investigations, such as thermal expansion and Raman measurements, paint a murkier picture.[8,9] A low-temperature structural study is still missing.

β′-(ET)$_2$SF$_5$CF$_2$SO$_3$ belongs to a special family of ET-based organic molecular conductors. These compounds contain a highly tunable molecular counterion complexed with the ET building block to form a salt with β′ packing, as shown in Figure 1. β′-Packing is a fairly rare packing motif, very different from the packing configuration of β″ materials. In β′-packing, the planes of the ET molecules are arranged perpendicular to the stacking axis, whereas in β″, the planes of the ETs are slightly canted with respect to the stacking axis. Among the hundreds of known ET salts, only a few possess the β′ packing pattern.[10] The general formula for these organic molecular conductors is (ET)$_2$SF$_5$RSO$_3$; by chemically substituting various R groups, it is possible to stabilize a variety of different ground states.[11] Thus, the chemical tunability of this family of materials is extremely attractive. In systems with β′ packing, the anion $R = CF_2$ is predicted to give a SP material. Other β′-type solids include the β′-(ET)$_2$ X salts, where X = ICl_2^-, $BrICl^-$, or $AuCl_2^-$, are well-known counterions.[12,13] These systems are low-dimensional magnetic semiconductors that undergo antiferromagnetic (AFM) phase transitions between 20 and 30 K. Although optical methods have been used to study the electrodynamics of the β″materials[14−16] as well as other β′salts,[17] no such work has been carried out on β′-(ET)$_2$ SF$_5$CF$_2$SO$_3$.

To explore the nature of the low-temperature ground state in β′-(ET)$_2$SF$_5$CF$_2$SO$_3$, we have measured the polarized infrared reflectance as a function of temperature and calculated the optical constants from these data. We have also examined the spin-exchange interactions of this salt by performing a spin dimer analysis.[18−20]

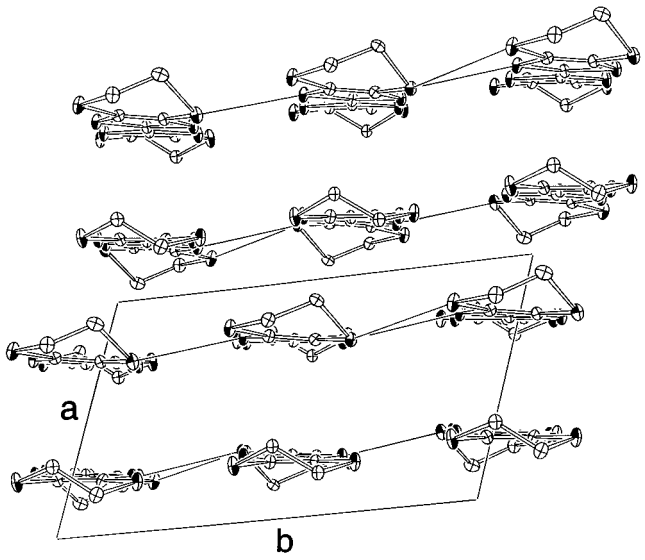

Figure 1. Crystal structure of β′-(ET)$_2$SF$_5$CF$_2$SO$_3$ in the *ab* plane. Note: the *a* -direction close to but not identical to the ⊥ *b* -direction (i.e. *a* and *b* are not orthogonal). The space group is $P\bar{1}$.

The objective of the present work is to search for evidence that will allow us to distinguish between the SP, AFM, and SG scenarios and understand the low-temperature electrodymanics in this material.

II. Experimental Section

High-quality single crystals of β′-(ET)$_2$SF$_5$CF$_2$SO$_3$ were grown electrochemically from the organic building block ET and LiSF$_5$CF$_2$SO$_3$ electrolyte in an H-cell at Argonne National Laboratory. The dimensions of the single crystal used for infrared measurements were 3.5 × 0.7 × 0.6 mm. The crystal structure of β′-(ET)$_2$SF$_5$CF$_2$SO$_3$ is triclinic and belongs to the space group $P\bar{1}$. The unit cell dimensions of this material are 7.862, 13.222, and 17.660 Å, for the *a*, *b*, and *c* directions, respectively; there are four ET molecules (two ET dimers) per unit cell. In the structure of β′-(ET)$_2$SF$_5$CF$_2$SO$_3$, ET molecules form vertical stacks in a β′ packing configuration (Figure 1). As is typical, the two-dimensional planes that make up the conducting donor layers are separated by layers of nonconducting counterions. The pathway of conductivity in this material is through the donor layer, and ET molecules form dimers with reasonable orbital overlap in the vertical stacking direction. Here, the $\vec{E} \parallel b$ polarization is the interstack direction, and the $\vec{E} \perp b$ polarization is close to the intrastack direction.[21]

Far and mid-infrared reflectance measurements were performed on a Bruker 113V with bolometer, photocell, and DTGS detectors over the 25−5000 cm^{-1} regime. Mylar beam splitters were used in the far-infrared region, and KBr was used for the mid-infrared. Additional far-infrared polarized reflectance measurements were taken at U10A infrared beamline at the National Synchrotron Light Source, Brookhaven Na-

(7) Ward, B. H.; Rutel, I. B.; Brooks, J. S.; Schlueter, J. A.; Winter, R. W.; Gard, G. L. *J. Phys. Chem. B*, submitted.
(8) Lang, M. Unpublished results.
(9) van Loosdrecht, P. H. M. Unpublished results.
(10) Mori, T. *Bull. Chem. Soc. Jpn.* **1998**, *71*, 2509.
(11) For example, in systems with β″ packing, R = CH_2CF_2 yields the first fully organic superconductor ($T_c \approx 5$ K).[14] An anion containing either R = $CHFCF_2$ or *R* = CHF gives a metal/insulator transition ($T_{MI} \approx 180$ K) or metallic material, respectively.[15,16] With the β″ materials, the chemical nature of the counterion is clearly important for stabilizing the uniquely different ground states.
(12) Emge, T. J.; Wang, H. H.; Leung, P. C. W.; Rust, P. R.; Cook, J. D.; Jackson, P. L.; Carlson, K. D.; Williams, J. M.; Whangbo, M.-H.; Venturini, E. L.; Schirber, J. E.; Azevedo, L. J.; Ferraro, J. R. *J. Am. Chem. Soc.* **1986**, *108*, 695.
(13) Emge, T. J.; Wang, H. H.; Bowman, M. K.; Pipan, C. M.; Carlson, K. D.; Beno, M. A.; Hall, L. N.; Anderson, B. A.; Williams, J. M.; Whangbo, M.-H. *J. Am. Chem. Soc.* **1987**, *109*, 2016.
(14) Dong, J. J.; Musfeldt, L.; Schlueter, J. A.; Williams, J. M.; Nixon, P. G.; Winter, R. W.; Gard, G. L. *Phys. Rev. B* **1999**, *60*, 4342.
(15) Olejniczak, I.; Jones, B. R.; Zhu, Z.; Dong, J.; Musfeldt, J. L.; Schlueter, J. A.; Morales, E.; Geiser, U.; Nixon, P. G.; Winter, R. W.; Gard, G. L. *Chem. Mater.* **1999**, *11*, 3160.
(16) Jones, B. R.; Olejniczak, I.; Dong, J.; Pigos, J. M.; Zhu, Z. T.; Garlach, A. D.; Musfeldt, J. L.; Koo, H.-J.; Whangbo, M.-H.; Schlueter, J. A.; Ward, B. H.; Morales, E.; Kini, A. M.; Winter, R. W.; Mohtasham, J.; Gard, G. L. *Chem. Mater.* **2000**, *12*, 2490.
(17) Kuroda, H.; Yakushi, K.; Tajima, H.; Ugawa, A.; Tamura, M.; Okawa, Y.; Kobayashi, A.; Kato, R.; Kobayashi, H.; Saito, G. *Synth. Met.* **1988**, *27*, A491.
(18) Whangbo, M.-H.; Koo, H.-J.; Lee, K.-S. *Solid State Commun.* **2000**, *114*, 27.
(19) Koo, H.-J.; Whangbo, M.-H. *J. Solid State Chem.* **2000**, *151*, 96.
(20) Koo, H.-J.; Whangbo, M.-H. *J. Solid State Chem.* **2000**, *153*, 263.
(21) Note the axes assignments for β′-(ET)$_2$SF$_5$CF$_2$SO$_3$ are the same as β″-(ET)$_2$SF$_5$RSO$_3$ materials. In these β″-type systems, the $E \parallel b$ polarization is defined as the interstack direction and $E \perp b$ polarization is the intrastack direction.

tional Laboratory. Here, a Bruker IFS 66v/s Interferometer with a liquid helium bolometer detector and various Mylar beam splitters were used to measure the far-infrared spectral range. Polarized optical reflectance measurements were made with a modified Perkin-Elmer λ-900 spectrometer in the 4800−33000 cm^{-1} energy range. This instrument is custom retrofit with a reflectance stage.

The optical axes of the crystal were determined as those displaying the greatest anisotropy at 300 K, and analysis of the structure shows good correspondence with the $\vec{E} \parallel b$ and $\vec{E} \perp b$ directions. For each polarization, infrared reflectance measurements were made at several temperatures between 10 and 300 K, concentrating around the proposed 45 K transition. Temperature control was achieved using an open-flow cryostat. For the optical range, data were collected only at 300 K.

Optical constants were obtained from a Kramers−Kronig analysis of the reflectance spectra. The complex dielectric function

$$\tilde{\epsilon}(\omega) = \epsilon_1(\omega) + i\epsilon_2(\omega) = \epsilon_1(\omega) + \frac{4\pi i}{\omega}\sigma_1(\omega) \qquad (1)$$

is obtained from the measured reflectance and the calculated phase shift integral; $\epsilon_1(\omega)$ is the real part of the dielectric function, and $\epsilon_2(\omega)$ is the imaginary part. Thus, $\epsilon_1(\omega)$ tells us how a material disperses energy, whereas $\epsilon_2(\omega)$ (or $\sigma_1(\omega)$) provides information on the lossy response. Our high-frequency data were extrapolated as ω^{-2}, and the low-frequency data were extrapolated to zero frequency as a constant, appropriate for a semiconducting material.[22]

PEAKFIT analysis was used to quantify the low-energy electronic excitation in the $\vec{E} \perp b$ direction. From the analysis, typical fit parameters of center frequency, line width and oscillator strength were extracted. A variety of line shapes were tested for suitability, including Gaussian, Lorenzian, and Voigt, with Voigt giving the most satisfactory results overall.[23] Errors (standard deviations) were estimated statistically based upon the results obtained from slightly different ranges of data and baselines.

III. Results

A. Room-Temperature Spectra. The 300 K reflectance spectrum of β'-$(ET)_2SF_5CF_2SO_3$ is shown in Figure 2 for the two principle polarization directions. The response is consistent with low-dimensional semiconducting behavior, with both strong vibrational features as well as low-lying electronic bands. Note that electronic excitations are present in both the $\vec{E} \parallel b$ (interstack) and $\vec{E} \perp b$ (intrastack) directions for the frequency range of 2000−6000 cm^{-1}. However, the band in the $\perp b$ direction is significantly more pronounced than that

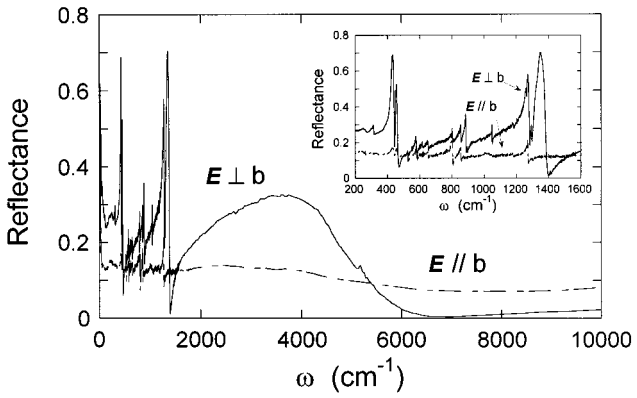

Figure 2. Room-temperature reflectance spectra of β'-$(ET)_2SF_5CF_2SO_3$ as a function of frequency. Solid line: $\vec{E} \perp b$ direction; dashed line: $\vec{E} \parallel b$ polarization. Inset: close-up view of the vibrational modes of β'-$(ET)_2SF_5CF_2SO_3$.

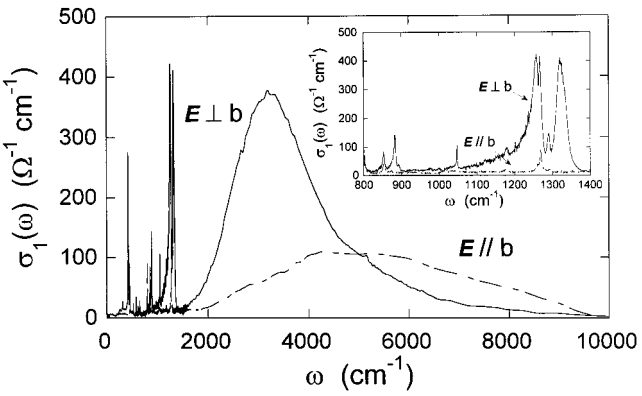

Figure 3. Room-temperature frequency-dependent optical conductivity of β'-$(ET)_2SF_5CF_2SO_3$ as a function of frequency. Solid line: $\vec{E} \perp b$ direction; dashed line: $\vec{E} \parallel b$ polarization. Inset: close-up view of the vibrational modes of β'-$(ET)_2SF_5CF_2SO_3$.

$\parallel b$. Vibrational structures are observed in both directions at low energy (inset of Figure 2), although these features are more prominent in the intrastack polarization. The marked differences in the vibration and electronic features between the two polarizations is an indication of the anisotropy of the material, a well-known ingredient of a SP transition. The electronic structure of β'-$(ET)_2SF_5CF_2SO_3$ is not, however, purely one-dimensional. The real part of the optical conductivity, $\sigma_1(\omega)$, calculated from the Kramer−Kronig analysis of the reflectance, is shown in Figure 3. Low-energy electronic excitations are clearly seen at 4000−6000 cm^{-1} and 3200 cm^{-1} in both the $\vec{E} \parallel b$ and $\vec{E} \perp b$ directions, respectively.

Figure 4 shows the electronic band structure calculated for β'-$(ET)_2SF_5CF_2SO_3$ using the extended Hückel tight-binding method.[24,25] For simplicity, only the four highest occupied bands are shown, which result mainly from the highest occupied molecular orbitals (HOMOs) of the ET molecules. Since this salt is a magnetic semiconductor, all the levels of the upper band should be considered singly filled in band orbital representa-

(22) Wooten, F. *Optical Properties of Solids*; Academic Press: New York, 1972.

(23) $y = \dfrac{a_0 \int_{-\infty}^{\infty} \dfrac{\exp(-t^2)}{a_3^2 + \left(\dfrac{x - a_1}{a_2} - t\right)^2} dt}{\int_{-\infty}^{\infty} \dfrac{\exp(-t^2)}{a_3^2 + t^2} dt}$ where a_0 = amplitude, a_1 = center, a_2 = width, and a_3 = shape.

(24) Whangbo, M.-H.; Hoffmann, R. *J. Am. Chem. Soc.* **1978**, *100*, 6397.

(25) Our calculations were carried out using the CAESAR program package (Ren, J.; Liang, W.; Whangbo, M.-H. Crystal and Electronic Structure Analysis Using CAESAR, 1998. This book can be downloaded free of charge from the web site http://www. PrimeC.com/.)

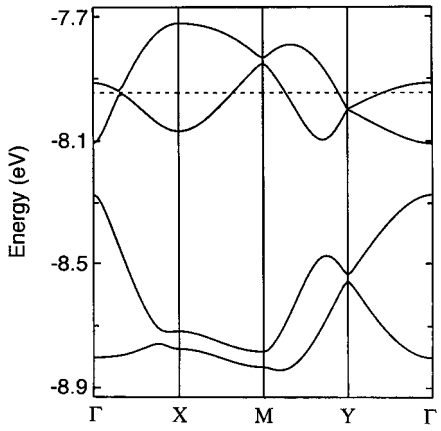

Figure 4. Dispersion relations of the four highest occupied bands calculated for β′-(ET)$_2$SF$_5$CF$_2$SO$_3$, where the Fermi level (the horizontal dashed line) is given assuming that the salt is metallic. Here, $\vec{E} \perp$ and $\vec{E} \parallel b$ polarizations are equivalent to the Γ → X and Γ → Y directions, respectively.

tion.[26] A possible optical excitation predicted for β′-(ET)$_2$SF$_5$CF$_2$SO$_3$ from the electronic band structure is the interband transition, i.e., the $\psi_+ \rightarrow \psi_-$ excitation. This transition is consistent with the broad and weak absorption in the optical conductivity along the $\vec{E} \parallel b$ direction in Figure 3. The strong and sharp $\vec{E} \perp b$ excitation centered at 3200 cm^{-1} in Figure 3 is not adequately explained in terms of the electronic band structure. It originates most likely from an electron-hopping (charge-transfer) excitation from the singly filled ψ_- level of one $(ET)_2^+$ dimer cation to that of its neighboring dimer cation. The excited-state associated with this transition leads to an electron pairing in one ψ_- level and hence causes on-site Coulomb repulsion, U. If it is assumed that the excitation energy is due solely to U, its value is estimated to be about 0.4 eV from the fact that the absorption peak is centered at 3200 cm^{-1}. Actually, many organics fall into the category $U \sim 4t$, instead of having large or small U. In the large U limit, electron−electron interactions are important and localized models are necessary, whereas band structure is more appropriate for small U.

Using the Sommer model,[27] the experimental value of the screened plasma frequency $\tilde{\omega}_p = \omega_p/\sqrt{\epsilon_\infty} \sim 4826$ cm^{-1},[28] and an inner dimer separation of 3.9 Å, we estimate the hopping integral (t) for β′-(ET)$_2$SF$_5$CF$_2$SO$_3$ to be $t \approx 2800$ cm^{-1} in the $\vec{E} \perp b$ direction. This estimate is consistent with the electronic band structure calculations (Figure 4), as well as the $\vec{E} \perp b$ electronic excitation shown in Figure 3.[29]

Many of the low-energy vibrational features displayed in the inset of Figure 3 can be identified as the totally symmetrical A$_g$ modes of the ET molecule. Here, the normally infrared-inactive A$_g$ modes are activated by coupling with the aforementioned low-lying electronic transitions, and they appear at perturbed frequencies in $\sigma_1(\omega)$ relative to Raman results.[30−32] These structures will be discussed in more detail in the next Section. The normally infrared-active modes of ET$^{+0.5}$ [30−32] and $SF_5CF_2SO_3^-$ anion [33,34] are observed in the spectra of β′-(ET)$_2$SF$_5$CF$_2$SO$_3$ as well.

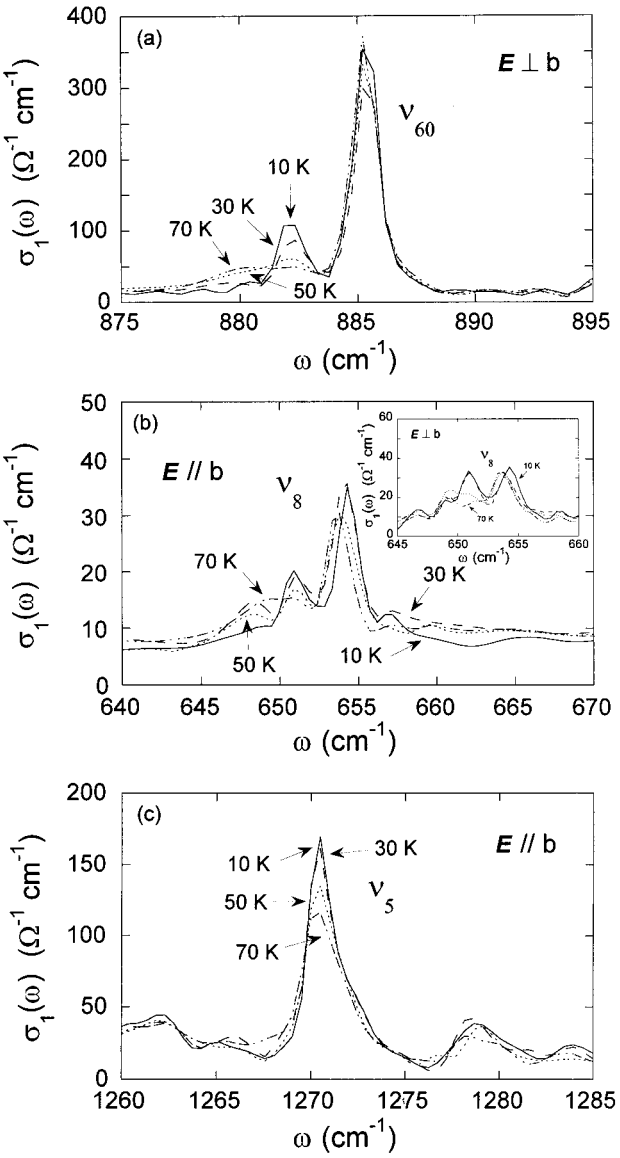

Figure 5. Temperature-dependent optical conductivity of β′-(ET)$_2$SF$_5$CF$_2$SO$_3$ at 10, 30, 50 and 70 K. (a) ν_{60} $\vec{E} \perp b$ in the direction; (b) ν_8 in the $\vec{E} \parallel b$ direction; the inset of (b) ν_8 in the $\vec{E} \perp b$ direction; (c) ν_5 in the $\vec{E} \parallel b$ direction.

B. Temperature Dependence. 1. Vibrational Properties. Figure 5 displays a close-up view of several key vibrational modes of β′-(ET)$_2$SF$_5$CF$_2$SO$_3$ in the temperature-dependent optical conductivity. The spectra taken at 10, 30, 50, and 70 K bracket the 45 K transition, and the modes of interest are ν_{60} (B_{3g}), ν_8 (A_g), and ν_5 (A_g). In Figure 5a, the $\vec{E} \perp b$ response of ν_{60} (electron−phonon activated C−S stretching mode) ex-

(26) Whangbo, M.-H. *J. Chem. Phys.* **1979**, *70*, 4963.
(27) Sommer, W.; Moldenhauer, J.; Schweiter, D.; Heinen, I.; Keller, H. J. *Synth. Met.* **1995**, *68*, 133.
(28) Jacobsen, C. S. *Semiconductors and Semimetals*; Cornwell, E. M., Ed.; Academic Press Inc.: New York, , 1985; Vol. 27, Chapter 5.
(29) In the $\vec{E} \parallel b$ direction, we cannot estimate t using this model because $\epsilon_1(\omega)$ does not cross zero.
(30) Eldridge, J. E.; Homes, C. C.; Williams, J. M.; Kini, A. M.; Wang, H. H. *Spectrochim. Acta A* **1995**, *51*, 947.
(31) Eldridge, J. E.; Xie, Y.; Wang, H. H.; Williams, J. M.; Kini, A. M.; Schlueter, J. A. *Spectrochim. Acta A* **1996**, *52*, 45.
(32) Eldridge, J. E.; Xie, Y.; Lin, Y.; Homes, C. C.; Wang, H. H.; Williams, J. M.; Kini, A. M.; Schlueter, J. A. *Spectrochim. Acta A* **1997**, *53*, 565.
(33) Hamel, N. N.; Nixon, P. G.; Gard, G. L.; Nafshun, R. L.; Lerner, M. M. *J. Fluorine Chem.* **1996**, *79*, 81.
(34) Gard, G. L.; Waterfeld, A.; Mews, R.; Mohtasham, J.; Winter, R. *Inorg. Chem.* **1990**, *29*, 4588.

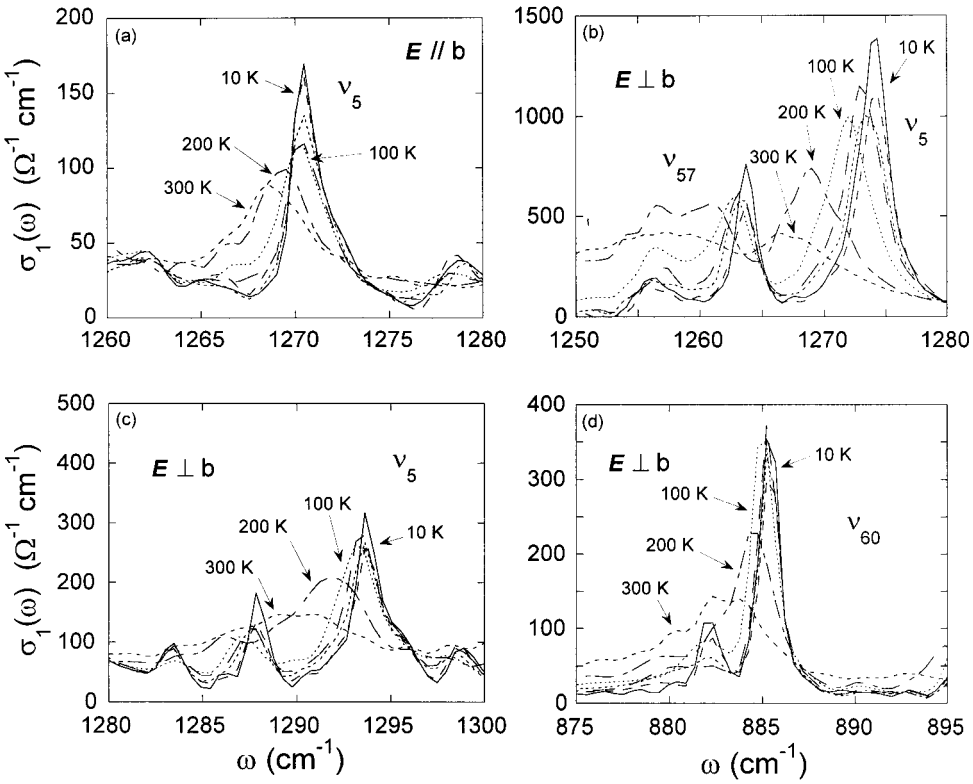

Figure 6. Temperature-dependent optical conductivity of β'-$(ET)_2SF_5CF_2SO_3$ at 10, 30, 50, 70, 100, 200, and 300 K. (a) ν_5 in the $\vec{E} \parallel b$ direction; (b) ν_{57} and ν_5 in the $\vec{E} \perp b$ direction; (c) another component of ν_5 in the $\vec{E} \perp b$ direction; (d) ν_{60} in the $\vec{E} \perp b$ direction.

hibits a doublet structure at 10 and 30 K, whereas above the 45 K transition, there is little or no presence of the doublet. In Figure 5b, the $\vec{E} \parallel b$ component of ν_8 (electron−phonon activated C−S stretching) shows a noticeable change in intensity between 30 and 50 K. At the same time, ν_8 in the $\vec{E} \perp b$ direction (inset of Figure 5b) has behavior similar to ν_{60}, with a weak doublet structure below 45 K. Again, there is little or no presence of the doublet above the transition temperature. In Figure 5c, ν_5 (electron−phonon activated H−C−C and H−C−H bending) in the $\vec{E} \parallel b$ direction displays a nonmonotonic change in oscillator strength between 30 and 50 K, the same behavior as ν_8.

Important high-temperature modifications are also seen in the vibrational modes of β'-$(ET)_2SF_5CF_2SO_3$, as shown in Figure 6. The spectra over a wide range of temperatures (10−300 K) illustrate a nonmonotonic frequency shift between 100 and 200 K; the behavior of ν_5 (A_g) (both in $\vec{E} \parallel b$ and $\vec{E} \perp b$ directions), ν_{57} (B_{3g}), and ν_{60} (B_{3g}) is representative. The physical nature of ν_5 and ν_{60} were described previously as electron−phonon activated H−C−C/H−C−H bending and C−S stretching, respectively; ν_{57} is electron−phonon activated H−C−C, H−C−H and H−C−S bending. In Figure 6 (a), the $\vec{E} \parallel b$ response of ν_5 (electron−phonon activated H−C−C and H−C−H bending) displays noticeable shifting between 100 and 200 K. In Figure 6b, both ν_{57} (H−C−C and H−C−S bending mode) and the $\vec{E} \perp b$ component of ν_5 display two different trends in this temperature regime. ν_5 (centered at 1268 cm^{-1}) shows the same red-shifting as ν_5 (in the $\vec{E} \parallel b$ direction) with increasing temperature (Figure 6a); whereas ν_{57} (near 1257 cm^{-1}) demonstrates prominent splitting below 200 K. In Figure 6c, another portion of the ν_5 mode in the $\vec{E} \perp b$ direction exhibits a distinct doublet structure at 100 K.

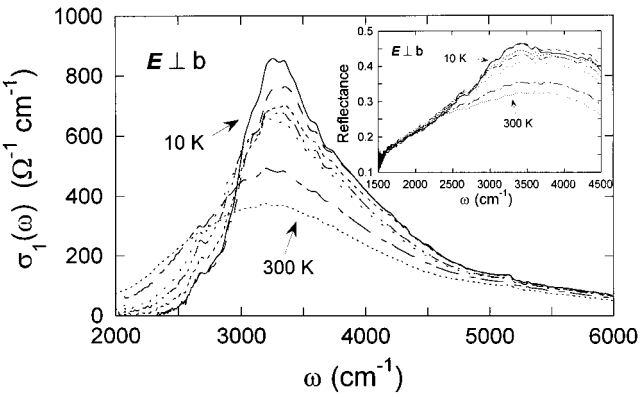

Figure 7. Close-up view of the low-lying electronic excitation in the optical conductivity of β'-$(ET)_2SF_5CF_2SO_3$ in the $\vec{E} \perp b$ direction at 10, 30, 50, 70, 100, 200, and 300 K. Inset: reflectance of β'-$(ET)_2SF_5CF_2SO_3$ in the $\vec{E} \perp b$ polarization between 10 and 300 K. Temperature is decreasing in sequential order with increasing spectral intensity.

Above 200 K, the doublet structure has dissipated and the feature is noticeably broadened. In Figure 6d, ν_{60} (C−S stretching mode) in the $\vec{E} \perp b$ direction displays narrowing and frequency-shift that saturates at 100 K. As discussed in a later Section, these frequency shift trends are likely related to another higher temperature transition.

2. Electronic Structure. Figure 7 shows a close-up view of the mid-infrared $\vec{E} \perp b$ optical conductivity of β'-$(ET)_2SF_5CF_2SO_3$ as a function of temperature. The low-energy electronic excitation (centered at 3200 cm^{-1}) shows distinct changes with temperature that are consistent with the aforementioned trends in vibrational structure, pointing toward transitions at 45 K and between 100 and 200 K. First, there is a small non-

monotonic intensity decrease of the charge-transfer band (near the peak frequency of 3200 cm^{-1}) between 30 and 50 K. Second, the excitation shows a very clear level change between 100 and 200 K, as well as a noticeable increase in width. The trends described above are easily observed in the reflectance data of β′-(ET)$_2$SF$_5$CF$_2$SO$_3$ as well (inset of Figure 7) and may be connected with a change in electronic overlap within the dimer, likely caused by a small relative shift or displacement of the two ET$^{+0.5}$ molecules.

We quantify these trends using PEAKFIT analysis, from which we extract typical fit parameters such as center frequency, line width, and oscillator strength. At room temperature, three Voigt oscillators are needed for the fit. That three oscillators are appropriate (and essential) to mimic this structure becomes more obvious as temperature is lowered. We concentrate on the parameters that change at the 45 and 100−200 K phase boundaries. Figure 8a displays the center frequency as a function of temperature for the three oscillators. Oscillator 2 is the most sensitive to the 45 K transition. In Figure 8b, changes in line width near 45 K are best shown by oscillators 1 and 3, both with notable line width narrowing before the transition. In addition, oscillators 1 and 2 show substantial line width variation between 100 and 200 K that is directly observable in the optical conductivity (Figure 7). Finally, in the plot of total oscillator strength (Figure 8c), modes 1 and 2 show a change in slope through 45 K. The trends in the latter case are very pronounced and include a range of temperatures leading to the transition, indicative of some possible fluctuation effects. No substantial changes in oscillator strength can be identified in the 100−200 K region.

IV. Discussion

A. Low-Temperature (45 K) Transition. The 45 K transition in β′-(ET)$_2$SF$_5$CF$_2$SO$_3$ is characterized by a number of small but distinct changes in the infrared and low-energy electronic response. We consider in turn several possible explanations for this behavior, combining our results with previous measurements, to identify a mechanism that supports our findings.

Considering the close chemical and structural relationship between β′-(ET)$_2$SF$_5$CF$_2$SO$_3$ and a number of prototypical AFM organic solids,[12,13] it is attractive to consider this model at the outset. In support of AFM ordering, the anisotropic low-lying electronic excitations observed in Figure 3 are typical of a highly correlated system.[35,36] However, low-temperature ESR line widths and susceptibilities change isotropically at 45 K;[6,7] an anisotropic response is an essential signature of the AFM transition. Further, no change in vibrational or low-lying electronic structures is expected below 45 K due to the absence of a lattice distortion within the AFM framework. Clearly, β′-(ET)$_2$SF$_5$CF$_2$SO$_3$ deviates substantially from this picture, and we can rule out an AFM ground state below 45 K.

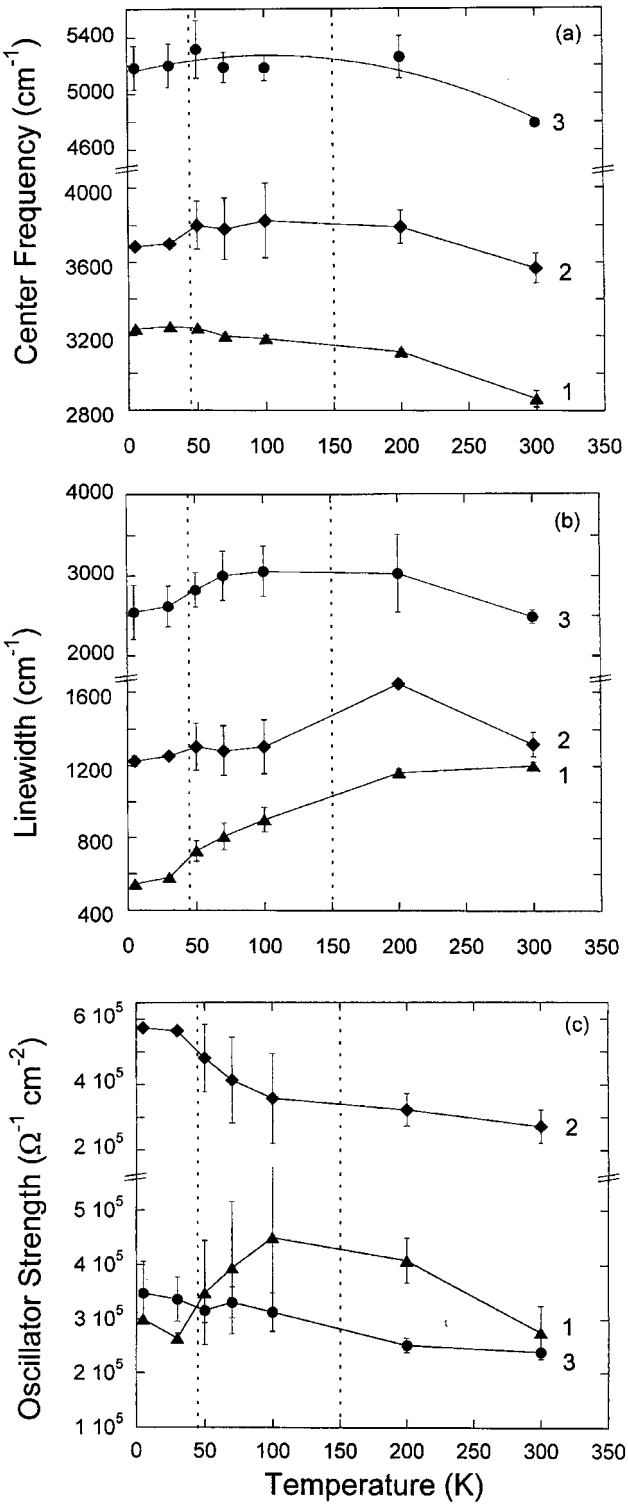

Figure 8. (a) Center frequency as a function of temperature for β′-(ET)$_2$SF$_5$CF$_2$SO$_3$ (b) The line width response as a function of temperature. (c) The oscillator strength as a function of temperature for the three oscillators of interest. Here △ − oscillator 1, ◇ − oscillator 2, and ○ − oscillator 3.

Second, we consider β′-(ET)$_2$SF$_5$CF$_2$SO$_3$ as a possible SG material, where the spin gap opens without an accompanying lattice distortion. Examples include CaV_2O_5 and MgV_2O_5;[37] no structural change has been identified in either of these compounds, hence the classification as SG rather than SP. Based on ESR line width and susceptibility results, β′-(ET)$_2$SF$_5$CF$_2$SO$_3$

(35) Dressel, M.; Schwartz, A.; Grüner, G.; Degiorgi, L. *Phys. Rev. Lett.* **1996**, *77*, 398.
(36) Degiorgi, L.; Dressel, M.; Schwartz, A.; Alavi, B.; Grüner, G. *Phys. Rev. Lett.* **1996**, *76*, 3838.
(37) Ueda, Y. *Chem. Mater.* **1998**, *10*, 2653, and references therein.

certainly displays a SG; however, β'-$(ET)_2SF_5CF_2SO_3$ also shows changes in vibrational as well as electronic structures near 45 K that support weak lattice involvement in the transition. This suggests that the low-temperature ground state is more complex and that an isolated SG model cannot provide a complete explanation for the properties of β'-$(ET)_2SF_5CF_2SO_3$ at low temperature.

Third, we consider the SP mechanism as applied to β'-$(ET)_2SF_5CF_2SO_3$.[38] We have observed low-temperature modifications in a number of vibrational features that are consistent with a weak elastic distortion at 45 K (Figure 5). Note that these modes are observed in both the $E \parallel b$ and $E \perp b$ polarizations. This can be understood if the dimerization direction of the SP transition is along the $(-a + b)$ diagonal, as discussed below. In addition, there is a weak variation in the charge-transfer band through the transition that provides further evidence of a displacement in the stack ($E \perp b$) direction (Figure 7). This weak elastic distortion, combined with the presence of a SG inferred from previous ESR measurements,[6,7] points toward the SP mechanism as the best candidate at this time for describing the low-temperature phase of β'-$(ET)_2SF_5CF_2SO_3$.

As mentioned previously, diagonal spin pairing is indicated by calculations of spin−orbital interaction energies. The strength of an AFM spin-exchange interaction between two adjacent spin sites becomes large with increasing spin−orbital interaction energy, Δe.[18−20] Since a spin site of β'-$(ET)_2SF_5CF_2SO_3$ is given by an $(ET)_2^+$ dimer cation, the spin−orbital interaction energy follows the energy split of the ψ_- level in the spin dimer, i.e., two adjacent $(ET)_2^+$ dimer cations, as depicted in Figure 9a. Our calculations of the spin−orbital interaction energies using the extended Hückel method show that the AFM spin-exchange interaction along the $(-a + b)$ diagonal direction is stronger than that along the a direction by a factor of ≈ 4 and is stronger than that along the b direction by a factor of ≈ 2 (Figure 9(b)). Namely, the 1D AFM chains of β'-$(ET)_2SF_5CF_2SO_3$ run along the $(-a + b)$ diagonal direction, and hence the dimerization of the SP transition is anticipated along the $(-a + b)$ diagonal direction. This theoretical result is consistent with the above experimental observation, although the coupling direction differs from that observed in high field ESR.[7]

B. High-Temperature Transition. In β'-$(ET)_2SF_5CF_2SO_3$, both infrared and low energy electronic spectroscopies point to distinct changes between 100 and 200 K. Temperature-dependent ESR line width measurements (not shown) further support this finding with a nonmonotonic line width response around 150 K.[39] Below, we discuss several possible mechanisms for the 100−200 K transition including: a structural phase transition, ordering of the terminal ethylene groups, order/disorder effects in the $SF_5CF_2SO_3^-$ counterion, and charge ordering (CO) behavior.

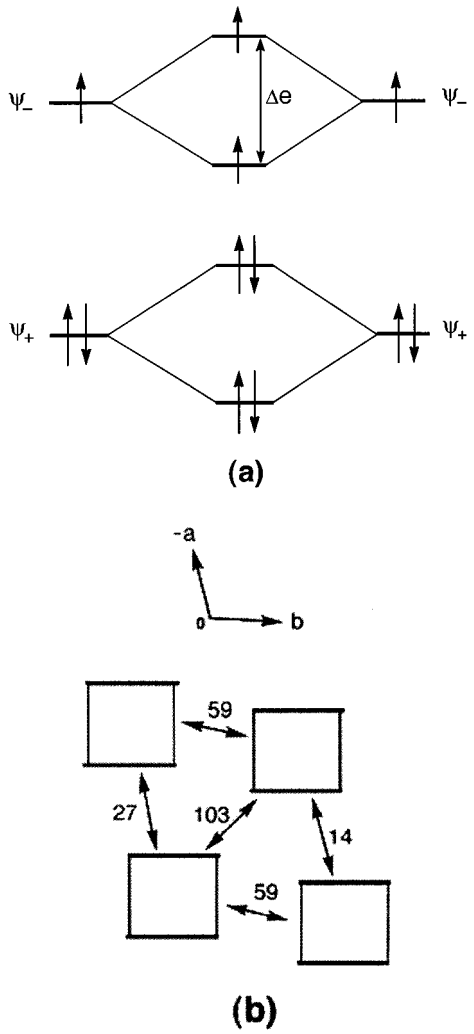

Figure 9. (a) Orbital interaction between two adjacent $(ET)_2^+$ dimers of β'-$(ET)_2SF_5CF_2SO_3$ leading to the spin−orbital interaction energy, Δe. (b) Calculated spin−orbital interaction energies (in meV) between adjacent $(ET)_2^+$ dimer cations.

Structural measurements have been performed on β'-$(ET)_2SF_5CF_2SO_3$ through the proposed 150 K transition.[40] We find minimal changes in the unit cell parameters (α, β, γ, a, b and c), the strongest being only an inflection point, indicating that the high temperature transition has a very weak (if any) long-range structural component. The observed frequency shifts are fairly substantial (on the order of 1−3 cm^{-1}), so it is unlikely they are solely attributable to a structural transition.

A second possible mechanism for the high-temperature transition is the subtle ordering of the ethylene end groups on the ET molecule through the 100−200 K regime.[41,42] If such a model is appropriate for β'-$(ET)_2SF_5CF_2SO_3$, then only the ethylene-related vibrational modes ought to show enhanced (or different) behavior through the 100−200 K temperature range. We observe changes in a majority of modes through 150 K, however, including those of primarily nonethylene end group origin. For example, in Figure 6d, ν_{60} (which is dominantly a C−S stretching mode) displays a similar

(38) Interactions of the lattice distortion with the spin chain are expected to be weak in a molecular solid, and only modest changes are anticipated through the transition; further, changes will not necessarily be observed for all vibrational modes.

(39) Ward, B. H.; Schlueter, J. A.; Geiser, U.; Wang, H.-H.; Morales, E.; Parakka, J. P.; Thomas, S. Y.; Williams, J. M. Unpublished results.

(40) Geiser, U. Unpublished results.

(41) Müller, H.; Madsen, D.; Wanka, S.; Wosnitza, J. *Synth. Met.*, submitted.

(42) Müller, H.; Madsen, D.; Fitch, A. N.; Wanka, S.; Wosnitza, J. *J. Physique IV* **2000**, *10*, 147.

frequency shift with temperature as ν_5 (Figure 6c) in the $\vec{E} \perp b$ polarization. That the large frequency shift is not exclusive for the ethylene-related vibrational modes suggests that an order/disorder mechanism involving the ethylene end groups is not the sole driving force of the 100−200 K transition in β′-(ET)$_2$SF$_5$CF$_2$SO$_3$, although we cannot rule out such participation altogether because of mode mixing effects.

Counterion ordering is a well-known factor in a number of low-temperature phase transitions in organic solids.[43,44] However, counterion modes in β′-(ET)$_2$SF$_5$CF$_2$SO$_3$ do not show splitting or any change in character through the 100−200 K regime, indicating that counterion ordering is not a dominant factor here, in contrast to results on related β″ systems.[16]

The lack of both substantial structural changes and evidence for more subtle ethylene or counterion ordering suggests that we should look elsewhere for an understanding of the 100−200 K transition in β′-(ET)$_2$SF$_5$CF$_2$SO$_3$. Recent theoretical work predicts the occurrence of CO in organic molecular solids; there are various possible charge distributions in quarter-filled low-dimensional salts.[45] This theoretically predicted charge disproportionation is supported by recent experimental work in several prototype materials,[46−50] and may be a possibility in β′-(ET)$_2$SF$_5$CF$_2$SO$_3$. For instance, it is well-known that CO forms a phase boundary "line" on the generalized T−P phase diagram of TMTTF and TMTSF materials.[47] The presence of CO coupled with magnetic ordering has also been identified in α′−NaV$_2$O$_5$.[50] In this material, the CO is virtually superimposed on the spin gap opening. This pattern of a high-temperature CO transition preceding a magnetically driven transition is an interesting area for further investigation.

V. Conclusion

The polarized infrared reflectance of β′-(ET)$_2$SF$_5$CF$_2$SO$_3$ has been measured as a function of temperature. Vibrational splitting as well distinct changes in the electronic structure below the 45 K transition indicate that a weak lattice distortion accompanies SG formation in this material, supporting a SP phase transition mechanism. The spin−orbital interaction energies calculated for this salt predict that the 1D AFM chains run along the (−*a* +*b*) diagonal direction, so the dimerization associated with the SP transition should occur along the (−*a* +*b*) direction, consistent with the polarization-dependent vibrational response. Additionally, we identify a second transition between 100 and 200 K and discuss the possible origin as a structural, order/disorder, or charge ordering type.

Acknowledgment. This project was supported at SUNY-Binghamton by Grant No. DMR-9623221 from the Division of Materials Research at the National Science Foundation. Research carried out at the National Synchrotron Light Source at Brookhaven National Laboratory was supported by the Department of Energy under Contract No. DE-AC02-98CH10886. Work at North Carolina State University and Argonne National Laboratory was supported by the Office of Basic Energy Science, Division of Material Sciences, U.S. Department of Energy, under Grants DE-FG05-86ER45259 and W-31-109-ENG-38. Research at Portland State University was supported by NSF grant No. CHE-9904316 and the Petroleum Research Fund ACS-PRF 34624-AC7. This work has benefitted from useful conversations with J.S. Brooks, D.K. Campbell, R.T. Clay, S. Mazumdar, I. Olejniczak, and V. M. Yartsev.

CM000839D

(43) Baker, S. M.; Dong, J.; LI, G.; Zhu, Z.; Musfeldt, J. L.; Schlueter, J. A.; Kelly, M. E.; Daugherty, R. G.; Williams, J. M. *Phys. Rev. B* **1999**, *60*, 931.

(44) Liu, H.-L.; Chou, L.-K.; Abboud, K. A.; Ward, B. H.; Fanucci, G. E.; Granroth, G. E.; Canadell, E.; Meisel, M. W.; Talham, D. R.; Tanner, D. B. *Chem. Mater.* **1997**, *9*, 1865.

(45) Mazumdar, S.; Clay, R. T.; Campbell, D. K. *Phys. Rev. B* **2000**, *62*, 13400.

(46) Miyagawa, K.; Kawamoto, A.; Kanoda, K. *Phys. Rev. B* **2000**, *62*, R7679.

(47) Bourbonnais, C.; Jerome, D. *Science* **1998**, *281*, 1155.

(48) Chow, D. S.; Zamborszky, F.; Alavi, B.; Tantillo, D. J.; Baur, A.; Merlic, C. A.; Brown, S. E. *Phys. Rev. Lett.* **2000**, *85*, 1698.

(49) Coulon, C.; Parkin, S. S. P.; Laversanne, R. *Phys. Rev. B* **1985**, *31*, 3583.

(50) Fagot-Revurat, Y.; Mehring, M.; Kremer, R. K. *Phys. Rev. Lett.* **2000**, *84*, 4176.